# IR Vaporization Mass Spectrometry of Aerosol Particles with Ionic Solutions: The Problem of Ion−Ion Recombination

**Yury Dessiaterik, Theresa Nguyen, Tomas Baer,* and Roger E. Miller**

*Department of Chemistry, University of North Carolina, Chapel Hill, North Carolina 27599-3290*

*Received: July 24, 2003; In Final Form: October 9, 2003*

Rapid laser-induced thermal ablation of aerosol particles can result in the ejection of desolvated ions into the gas phase. In an effort to understand this phenomenon, we have carried out studies of ethylene glycol droplets containing $10^{-6}$ and $10^{-1}$ M RbCl. A high-power infrared $CO_2$ laser pulse vaporized the aerosol particles, and the resulting ions were detected by time-of-flight mass spectrometry and by total current measurements. The absolute number of ions in the particle was varied by controlling the size and the concentration of the ions in the particles. The results show that, at low concentrations, the ion signal is directly proportional to the ion concentration, whereas the signal saturates above $10^{-4}$ M RbCl. By comparing the TOF signal to the total current measured on the ion repeller plate, we were able to determine that ion−ion recombination is the major cause of this signal saturation. The ion collection efficiency of the TOF mass spectrometer at low ion concentration, where ion−ion recombination is not important, was found to be 5%. An ion−ion recombination model, developed by Langevin and Thomson, was found to accurately reproduce the measured ion collection efficiencies for various particle sizes, as well as ion concentrations ranging over 4 orders of magnitude.

## Introduction

A recent investigation from our laboratory of base-catalyzed nitromethane combustion involved rapid infrared heating of aerosol particles, consisting of neat nitromethane with trace amounts of base.[1] The single aerosol particles were accelerated toward the ionization region of a time-of-flight mass spectrometer, where they were rapidly heated to well above 2000 K. The neutral species produced in this reaction were ionized by a vacuum ultraviolet (VUV) laser and mass analyzed by their ion time-of-flight (TOF). On the other hand, the ionic species in solution, resulting from trace amounts of diethylamine (the base), could be detected in the mass spectra without ionization by the VUV laser. Because the ions originating from the VUV laser ionization of neutral species and the preexisting ions were created by entirely different mechanisms and at very different gas densities, it was not possible to relate the ion signals to their relative concentrations. This problem has led us to the current study in which we attempt to provide some understanding of the mechanism for ion liberation when a liquid droplet containing ions is suddenly vaporized. Studies of this type are also of interest for our current investigation of ionic liquids, such as ethyl-3-methylimidozolium nitrate. Among the attractive properties of ionic liquids are ease of storage, solubility, and low toxicity.

The quantitative measurement of ionic constituents is clearly an important issue that has been encountered by other workers as well.[2,3] A number of nontraditional ionization methods, including electrospray, thermospray, and MALDI, suffer from sensitivity variations as the analyte concentration is varied. At low concentrations, the signal intensity is typically linear with concentration, but saturates at high concentrations. The common feature in all of these experiments is the existence of the analyte in its ionic form in appreciable concentration, a situation that is very different from electron impact- or photoionization of a low-density gaseous target, where interaction between the ions is minimal. In addition, while electron impact generates primarily electrons and positive ions, the ablation of ionic species results in the formation of both positive and negative ions that strongly interact at high ion densities. Thus, the signal intensity in all of these methods can be depleted by ion−ion recombination, Coulomb explosion, and detector saturation, all of which are dependent on the density of ions. Recombination between positive and negative ions (referred to as precipitation in liquid nano droplets) has been suggested as the leading cause of electrospray signal saturation.[4] Once the ions of opposite charges have been separated by the applied electric field, ions of like charges repel one another to an extent that depends on the total ion concentration. This Coulomb explosion can impart several electronvolts of energy to the ions, thus making them difficult to transport into a mass spectrometer.[5]

In most experiments of the type discussed above, the precise cause of signal saturation is not readily determined owing to the difficulty in establishing the maximum possible signal. For instance, only a small fraction of the ions generated in electrospray pass through the small orifice and find their way into the mass spectrometer. In an effort to establish the relationship between the generation of charges and the final ion signal in electrospray, the total currents generated at the capillary and at the first skimmer were measured with an electrometer.[6] These studies show that, although the capillary current rises linearly with the ion concentration, the current measured at the skimmer saturates and even decreases when the ion concentration exceeds $10^{-4}$ M. The mechanism for ion generation is rather complex and involves partitioning of ions at the surface and in the bulk of the nano droplets,[2,4,7,8] so that the precise origin of the signal saturation is still not firmly established. Similar uncertainties are associated with saturation in MALDI and other laser ablation methods. Each laser shot ejects a microplasma of neutrals, positive and negative ions into the vacuum. A small and unknown fraction of the ions are eventually detected.[3,9−11]

10.1021/jp036171i CCC: $25.00 
Published on Web 11/22/2003

The effect of Coulomb explosion can be determined from the ions's translational energy, which can be measured from TOF peak widths or by measuring the ions' translational energy by electrostatic energy analyzers. However, translational energy in MALDI and other laser ablation experiments can arise from either Coulomb explosion or entrainment of the ions in the rapidly expanding plasma cloud. There is some evidence that the ion velocities are comparable to those of neutral species, which suggests that entrainment, rather than Coulomb explosion, may be the source of this translational energy.[3,12,13] This is consistent with the ejection of a relatively small number of ions in a large excess of neutral species. Thus, as in electrospray ionization, the MALDI process is complicated and as pointed out by Mansoori et al.[14] the "many interrelated factors influencing the MALDI signal intensity" make it "difficult to ascribe changes in the signal intensity to specific phenomena."

In the present work, we present results of an experiment in which the ionization process is considerably more controlled and thus provides an avenue for determining the source of signal saturation in laser-based aerosol time-of-flight mass spectrometry. The experimental approach involves complete laser vaporization of size-selected liquid aerosol droplets (2−5 $\mu$m) for a range of ion concentrations. In this way, the total number and density of ions not only are well established but also can be varied simply by changing the particle size and the ion concentration. Additionally, we employ a total ion current detector to accurately measure the number of ions released into the gas phase. Finally, we experimentally determine the maximum kinetic energies of the ions reaching the TOF detector. Our experimental results, although not directly applicable, are nevertheless relevant to MALDI and electrospray processes. They are most closely related to the laser desorption mass spectrometry of liquid beams and aerosol particles, in which an infrared laser is used to vaporize the aqueous phase, thus releasing the ions to the vacuum.[15−17]

## Experimental Approach

All of the experiments reported here were performed using a previously described aerosol time-of-flight mass spectrometer.[18] Aerosol particles are drawn into a collimating aerodynamic lens,[19,20] pass through two stages of differential pumping, which remove the suspending argon gas, and finally enter the main vacuum chamber. The expansion of the aerosol from the aerodynamic lens into the first stage of differential pumping accelerates the particles to a velocity that depends on their size. The particles enter the chamber at random times at a rate up to 10 per second and are detected by laser light scattering from two green diode lasers separated by 10 cm, which determines their velocity and thus also their size. When they arrive in the ionization region of the mass spectrometer, a $CO_2$ laser (triggered by the light scattering events) vaporizes the particle. The $CO_2$ laser power is kept high (∼500 mJ/pulse) to ensure rapid and complete particle vaporization. The laser beam was focused by a NaCl lens to a spot size of ∼1 mm. The bulk absorption coefficient for ethylene glycol was measured to be 19 $mm^{-1}$ by monitoring the absorption upon passing the laser beam through a 15 $\mu$m sample of pure ethylene glycol. In previous studies,[18] a second VUV laser was employed to ionize the vaporized neutral gas molecules. However, this was unnecessary in the present experiments because we are interested in detecting only the ions that already exist in solution. The ions are born in the center of a 2 cm extraction region (200 V/cm), which accelerates them to a second 0.50 cm acceleration stage (7.2 kV/cm), after which they pass through either a 15 cm or 1 m long drift region before being detected by a multichannel electron multiplier (Burle Electrooptics). The TOF spectrum for each particle is recorded using a digital oscilloscope (Infinium, Hewlett-Packard), and transferred to a computer. By adjusting the aerodynamic lenses alignment, it was possible to sample particles in narrow size distributions (5%), which were monitored by measuring the particle velocity. Most of the spectra presented here represent averages of 50 laser shots.

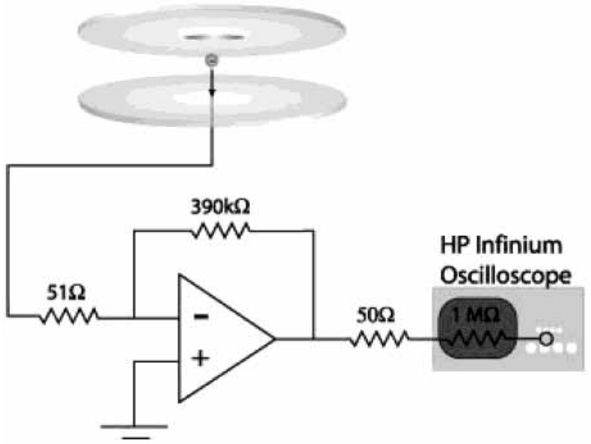


**Figure 1.** Electronic circuit for measuring the total ion current on the repeller plate. The purpose of the 50 Ω output resistor is to prevent self-exiting of the operational amplifier.

To establish absolute ion signals, the total ion current was collected on the repeller, using a Burr−Brown operational amplifier (OPA655u) in a current to voltage converter configuration. The circuit diagram for the converter employed is presented in Figure 1. The 7.5 cm diameter repeller plate lies 1 cm below the point of ionization. Its large surface area, combined with an applied electric field of 200V/cm, ensures that all of the negative ions (and electrons) that survive the evaporation process are collected; i.e., no ions are lost as a result of their initial kinetic energy. The grounded repeller plate was connected to the inverting input of the OPA655u through a 51 Ω resistor to prevent self-exciting of the operational amplifier. The op-amp output used a feedback loop through a 390 kΩ resistor and the output was read into the oscilloscope through a 1 MΩ resistor. This scheme allows an optimal reduction of noise for the measurement of incident current, by maintaining the repeller voltage at ground. The output voltage from the negative ions was recorded concurrently with the positive ion TOF spectrum. The time-dependent voltage was integrated and divided by the total resistance, to yield the total charge incident on the repeller plate. For example, for a typical integrated signal of 0.048 V $\mu$s, the number of collected ions ($7.7 \times 10^5$) is obtained by dividing the integrated signal by 390 kΩ and $1.6 \times 10^{-19}$ C/ion.

Solutions of RbCl (Aldrich) in ethylene glycol (Fisher) were prepared in concentrations ranging from $3 \times 10^{-7}$ to $3 \times 10^{-1}$ M. Particles ranging from 2 to 5 $\mu$m were produced by a nebulizer (Meinhard) using argon as a carrier gas.

## Results

**Signal Variation with Ion Concentration.** Figure 2 shows several time-of-flight (TOF) mass spectra obtained by IR laser-induced vaporization of RbCl-doped ethylene glycol aerosol droplets. These spectra were taken with a delayed pulse extraction field in order to generate narrow TOF peaks. RbCl was used in these studies (rather than NaCl) to avoid interference from the $Na^+$ impurity ions that were found in all aqueous and/

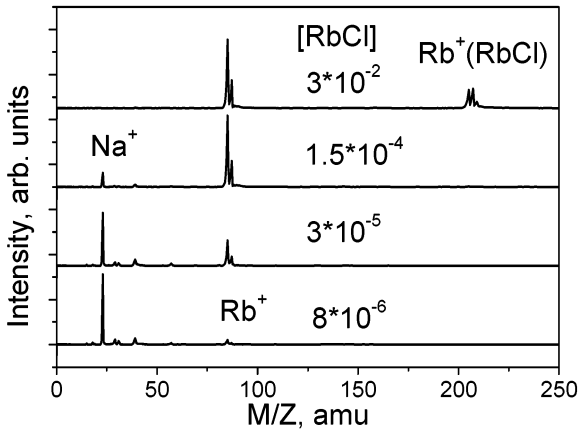


**Figure 2.** Typical positive ion TOF spectra of ethylene glycol aerosol droplets with various concentrations of RbCl. The mass spectra were obtained by vaporizing the droplet with a 500 mJ/pulse $CO_2$ IR laser. The $Na^+$ peaks are a result of contamination from the glass nebulizer. Pulsed delayed extraction was used to yield a narrow TOF peak.

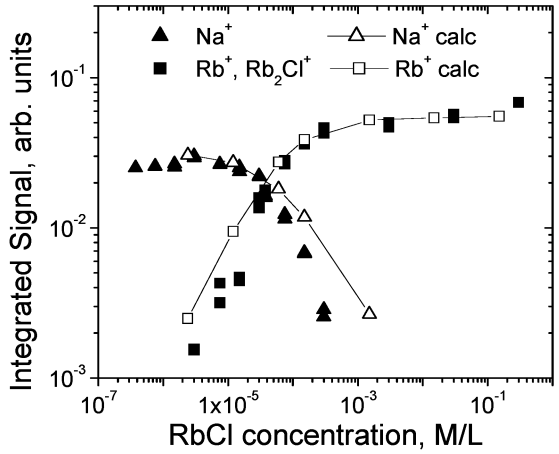


**Figure 3.** Integrated $Rb^+$ and $Na^+$ signals as a function of the RbCl concentration as measured on the multichannel plate detector at the end of a 1 m flight path. At low concentration, the signal rises linearly with the concentration. However, above a concentration of $2 \times 10^{-5}$ M, the signal saturates and the $Na^+$ signal decreases. The solid lines are calculated signals based on the Langevin/Thomson ion-recombination model assuming a particle diameter of 5 $\mu$m.

or ethylene glycol particles, presumably originating from the glass nebulizer used to generate the particles. At the lowest RbCl concentration of $3.2 \times 10^{-5}$ M, we see some low mass ions that are assigned to $H_3O^+$ (*m*/*z* 19), $Na^+$ (*m*/*z* 23), and $Na(H_2O)^+$ (*m*/*z* 41) as well as the $Rb^+$ peak at *m*/*z* 85. The $Rb^+$ signal increases slowly as the salt concentration is increased by 4 orders of magnitude. It is interesting to note that clusters become important only at the higher concentrations.

The integrated areas of the impurity signal and the rubidium ion peaks are shown in Figure 3. This clearly shows that, at low $Rb^+$ concentration, the observed $Rb^+$ signal increases in proportion to its concentration, while the $Na^+$ impurity signal remains constant. However, at concentrations above $3 \times 10^{-5}$ M RbCl, the $Na^+$ signal decreases (even though its concentration remains constant), and the $Rb^+$ signal begins to level off, or saturate. The implication is that the collection efficiencies for both the impurity $Na^+$ and the $Rb^+$ are decreasing over this ion concentration range. In fact, the $Na^+$ signal gives a direct measure of the collection efficiency. The reduced collection efficiency could be the result of a number of factors, including ion−ion recombination, Coulomb explosion (which reduces the

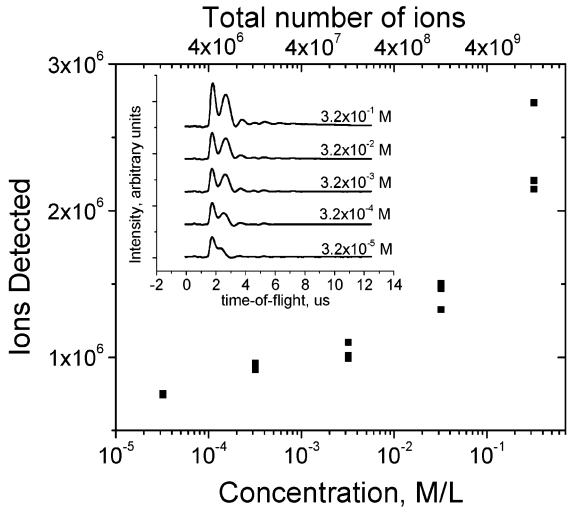


**Figure 4.** Total number of detected negative ions measured on the repeller plate as a function of the RbCl ion concentration (bottom scale) or the total number of ions (top scale). Note that the total signal (linear scale) increases by only a factor of 3.5 while the ion concentration increases by 4 orders of magnitude. The inset shows the ion current signals recorded on the operational amplifier.

collection efficiency for the high kinetic energy ions), and/or the saturation of the multichannel plate detector.

To determine the origin of the signal saturation in Figure 3, we collected the total ion current on the repeller plate using the circuit in Figure 1. Because this plate is located only 1 cm from the ionization region, all ions are collected, independent of their kinetic energy. In addition, signal saturation is not an issue for this detector. Figure 4 shows the resulting ion signal (linear scale) for various RbCl concentrations (log scale). The inset in this figure shows the time profile of the ion current at the repeller following laser vaporization. The 1 cm flight path is not sufficient to resolve ion masses. However, negative ion mass spectra collected with the 1 m drift region show that most of the negative ions are $Cl^-$ and $Cl(RbCl)^-$. The particle diameter was kept constant for all of these measurements at ~4.1 $\mu$m. While the concentration increases by 4 orders of magnitude, the number of ions collected at the repeller plate increases by only a factor of 3. The total ion current in Figure 4 (linear scale) closely follows the integrated ion signal in Figure 3 (log scale) measured at the end of the 1 m flight tube by the MCP detectors, implying that this saturation effect is a result of ion−ion recombination, rather then the loss of high-kinetic energy ions or detector saturation. Note that the lack of mass analysis on the repeller plate results in the measurement of the sum of the RbCl and the impurity NaCl signals.

Because we have measured the total ion current coming from a single 4.1 $\mu$m droplet, it is straightforward to compare the corresponding number of ions with the known number of ions in the solution. A 4.1 $\mu$m diameter droplet ($3.6 \times 10^{-14}$ L), with concentration of $3.2 \times 10^{-5}$ M RbCl, contains $7.0 \times 10^5$ $Rb^+$ ions. At this concentration the measured number of ions is $7.5 \times 10^5$, which is within the experimental uncertainty of the expected value. At higher concentrations the percentage of detected ions rapidly falls from 100% to 0.03%.

**Ion Recombination Model.** In this section, we apply the theory of ion recombination as outlined by Loeb[21] and Brown,[22] to aid in understanding the above data. In the high-density regime, Langevin[23] showed that the recombination rate is limited by diffusion and is thus inversely proportional to the pressure. In the low-density region, Thomson[24] demonstrated that the recombination is limited by the three body collisions rate,

making it proportional to the total gas density. As a result, the recombination rate passes through a maximum as the gas density increases.

In applying this model to the laser-induced vaporization of an aerosol droplet, we need to account for the rapidly varying gas density resulting from the expansion of the gas cloud. The simplest model for droplet evaporation assumes that the droplet is instantly vaporized upon IR laser irradiation and that the vapor cloud expands at the velocity of sound. Thus, we ignore the $CO_2$ laser pulse width of about 300 ns. We also assume that the density of vapor and ions within the cloud is uniform during this expansion. It is possible to take into account the radial dependence of the gas density using a model described by Zeldovich and Raizer,[25] although this would increase calculation time and it is not justified within accuracy of our model. The temperature of the gas cloud was assumed to be constant at 2000 K during the free expansion into the vacuum. This temperature is consistent with previous measurements of the translational temperature for other rapidly vaporized aerosol particles.[26] An accurate temporal variation of the translational temperature is not readily determined. As will become clear, the bulk of the ion−ion recombination takes place within 10 ns, while the gas density drops by a factor of about 100. If we assume isentropic adiabatic cooling and a calculated ethylene glycol heat capacity ($C_P$ at 2000 K) of 207 J/(mol K), the calculated temperature would decrease from 2000 to 1660 K, or a change of about 17%. On the other hand, if we were to relax the assumption of an infinitely short laser pulse, we would have to include laser heating of the gas during the expansion. Given these uncertainties, a constant temperature assumption is appropriate.

The assumption of instantaneous solvent loss is partly justified by power dependent studies and the use of various solvents. Whereas low laser powers used to evaporate aqueous ion droplets result in broad distributions of solvated ions, no such clusters are observed with an ethylene glycol solvent.

Ion−ion recombination can be described by the following kinetic equations:

$$\frac{dC_+}{dt} = \frac{dC_-}{dt} = -\alpha C_+ C_- \quad \text{and} \quad \frac{dC_i}{dt} = -\alpha C_i^2 \qquad (1)$$

where $C_- = C_+ = C_i$ are the concentrations of the negative and positive ions (assumed to be equal) and $\alpha$ is the recombination coefficient, which is a complicated function of the neutral gas density. According to the low-pressure Thomson model, $\alpha$ is proportional to the gas concentration (see Figure 5). The functional form at low pressures is

$$\alpha = \pi d_0^2 \sqrt{v_+^2 + v_-^2} f\left(\frac{2d_0}{\lambda}\right), \quad \text{with} \quad d_0 = \frac{1}{4\pi\epsilon_0}\frac{2e^2}{3kT} \qquad (2)$$

where $e$ is the electronic charge, $\lambda$ is the mean free path, and $v_+$ and $v_-$ are the thermal velocities of positive and negative ions, respectively. $d_0$ is defined as the distance between ions of opposite charge at which the potential energy, $e^2/d_0$, is equal to their relative kinetic energy, $^3/_2kT$. The function, $f$, is given by

$$f = 2w - w^2 \qquad (3)$$

$$w = 1 - \frac{2}{x^2}(1 - e^{-x}(x+1)) \quad \text{and} \quad x = \frac{2d_0}{\lambda}$$

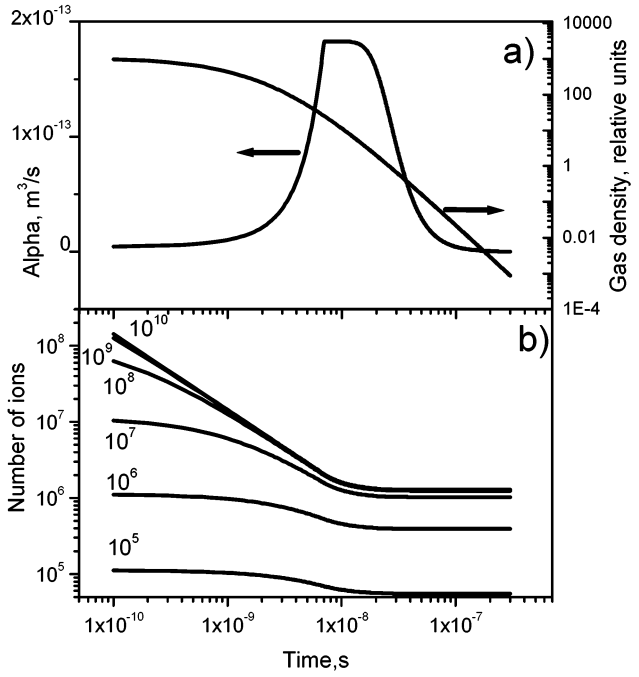


**Figure 5.** (a) Recombination coefficient, $\alpha$, and the neutral gas concentration as a function of time. The gas density is given in units of bar at room temperature. (b) Calculated number of ions in the vapor cloud based on the Langevin/Thomson ion-recombination model as a function of time after vaporization of the 5 $\mu$m aerosol droplet. The final ion concentrations after 20 ns are plotted in Figure 3.

According to the Langevin model, in the high-pressure regime, $\alpha$ is given by

$$\alpha = \frac{e}{\epsilon_0}(\mu_+ + \mu_-) \qquad (4)$$

where $\mu_+$ and $\mu_-$ are the mobilities of the positive and negative ions, respectively. The mobilities, and therefore the recombination rates, are inversely proportional to the neutral gas density in this pressure regime. The ion mobility, $\mu$, for a polarization interaction potential at 1 atm pressure in the low-temperature limit has been evaluated by McDaniel and Mason[27] as

$$\mu = \frac{13.87}{\sqrt{\alpha_p m_r}} \qquad (5)$$

where $\mu$ is in units of cm$^2$/(V s), $\alpha_p$ is the polarizability of gas molecules in A$^3$ (5.7 A$^3$ for ethylene glycol) and $m_r$ is the reduced mass of the ion and gas molecule in amu. We ignore the temperature dependence of the mobility, which is a function of the repulsive interaction potentials and does not vary by more than a factor of 2 over a broad temperature range.[27]

The important aspects of ion−ion recombination are the following. As two ions of opposite charges approach one another, their kinetic energy increases. However, if one of the ions collides with a neutral gas molecule, it will lose part of its kinetic energy. In the Thomson model, the energy following a collision is assumed to revert to the average energy, $^3/_2kT$. Recombination occurs when the kinetic energy of the ion after a collision with the neutral gas molecule is less than its potential energy ($e^2/r$) with respect to the nearest ion of opposite charge. At low pressures, the limiting step for ion recombination is the rate of collisions between the ions and neutral molecules, when the distance between the two ions is less than $d_0$. In this limit, the recombination coefficient is proportional to the pressure.

As pressure increases, the probability of a collision occurring when the ions are within a distance of $d_0$ increases and approaches unity, and the recombination coefficient approaches its maximum value. At higher pressures, the ion kinetic energy is no longer an issue, and the limiting step of recombination becomes the diffusion of the ion. In this region, the recombination coefficient is inversely proportional to the gas pressure.

The kinetic eq 1 was solved numerically using 100 ps time steps up to a total time of 300 ns, at which point the gas cloud has a diameter of about 600 $\mu$m. The calculations were performed for a particle diameter of 5 $\mu$m with various RbCl and NaCl concentrations. The variation of $\alpha$ during the course of expansion is shown in Figure 5a. At the moment of vaporization, the gas density is equivalent to a fluid at about 1000 bar, which diminishes within 300 ns by 6 orders of magnitude. $\alpha$ reaches its maximum value after about 7 ns, at which point the gas density is equivalent to a room-temperature pressure of 25 bar. Figure 5b shows the surviving number of ions for various ion concentrations as a function of time after the $CO_2$ laser vaporization pulse. It is evident that, independent of the initial ion concentration, recombination takes place during the first 20 ns, after which the ion and neutral gas densities are sufficiently low to prevent further recombination. During these first 20 ns, the diameter of the vapor cloud increases by a factor of about 8, corresponding to a 500-fold decrease in the gas density. The maximum recombination rate can be determined from the maximum slope in Figure 5b, which occurs at roughly 7 ns. It is most significant that for the high ion concentrations, the final ion count ($\sim 1.2 \times 10^6$) does not depend on the initial ion concentration and is rather close to the experimentally determined value. A more detailed model is not presently justified given that the exact temperature of the laser heated gas plume is not known. In fact, previous studies in our laboratory have suggested that the translational energy distribution of the expanding gas, resulting from high-power laser evaporation, is non-Boltzmann.[26]

This numerical calculation was then used to determine the signal level (remaining ions) as a function of the RbCl concentration in Figure 3. The calculation was normalized to the data at a RbCl concentration of $2 \times 10^{-2}$ M. Varying the assumed temperature from 2000 to 2400 K had little effect on the calculated results.

Because the final number of gas-phase ions is independent of the initial ion concentration in solution in the limit of high ion concentration, it should be possible to derive an equation that yields this final ion count without solving the kinetic equations numerically. If we assume that $\alpha$ is constant in time (i.e., independent of the gas density), the solution to eq 1 becomes

$$C(t) = \frac{C_0}{1 + C_0 \alpha t} \tag{6}$$

where $C_0$ is the initial ion concentration. For high initial ion concentrations, $C_0 \alpha t \gg 1$ and $C(t)$ is proportional to $(\alpha t)^{-1}$, which is indeed independent of the initial ion concentration. It is evident from Figure 5, that the bulk of the recombination takes place when $\alpha$ is close to its maximum value so that its value in eq 6 can be taken as $\alpha_{max}$, which can be determined from eq 2 with $f = 1$. The time in eq 6 represents the time during which the bulk of the recombination takes place. This $\Delta t$ can be estimated as the time required for the gas density to drop by a factor of 2 from its value where $\alpha$ is a maximum (between 7 and 10 ns in Figure 5). We can express this time in term of the velocity of the vapor cloud expansion $v_g$, the initial gas density $c_0$, the gas density when $\alpha$ reaches its maximum $c_{\alpha\,max}$, and the initial droplet diameter $D_0$, resulting in a final ion count $N_f$ given by

$$N_f = \frac{v_g}{\alpha_{max}} \left( \frac{c_0}{c_{\alpha\,max}} \right)^{2/3} D_0^2 \tag{7}$$

This equation yields the limiting number of surviving ions in the high ion concentration limit. For the case of a 5 $\mu$m diameter droplet, this number is $2.4 \times 10^6$. The measured final number of ions for this size droplet is about $2 \times 10^6$ ions. More importantly, this equation predicts that the final number of free ions is proportional to the square of the particle diameter. Although this equation is very approximate, the results for different particle diameters (presented later) are within a factor of 2 consistent with this prediction.

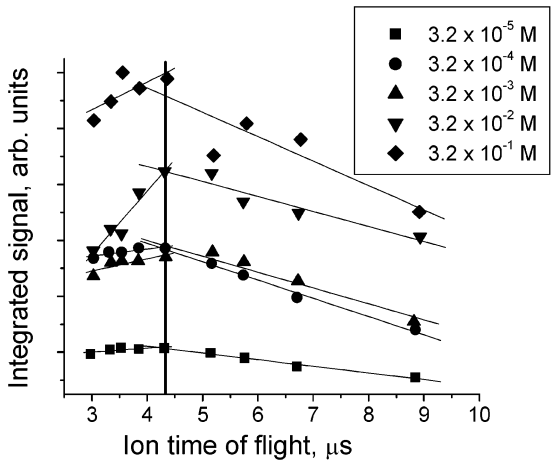


**Figure 6.** Integrated ion signal detected at the end of the 15 cm long TOF tube as a function of the total ion TOF, which was varied by changing the extraction and drift voltages for various ion concentrations. The decreasing signal as the flight time is increased is attributed to ion translational energy. Note that all detector signals peak at the same ion flight time, independent of initial ion concentration, which indicates that they have the same transverse translational energy.

**Ion Kinetic Energy.** The combination of the repeller experiment and the excellent agreement between the predictions of the recombination model and the data in Figure 3 shows that most of the signal loss can be attributed to ion recombination. Nevertheless, it is still worth considering the effects of the kinetic energy on the observed ion signal. The energy resulting from Coulomb repulsion of similarly charged ions causes a broadening of the ion TOF peak width. This provides a measure of the energy along the TOF extraction axis. Alternatively, it is also possible to obtain a measure of the initial ion translational energies perpendicular to the ion extraction axis by varying the ions' flight time by changing the accelerating electric field and the length of the drift tube. If ions are lost on the way to the detector because of their high kinetic energy, decreasing the flight time should reduce this loss. For example, a $Rb^+$ ion accelerated to 3 keV in a 1 m flight tube will miss the 2.5 cm multichannel plate detector if it possesses an original kinetic energy greater than 0.3 eV. Reducing the length of the drift tube to 15 cm reduces the ions' flight time and thus increases the maximum acceptable kinetic energy to 6 eV. Figure 6 shows the ion signal as a function of the ion time-of-flight, in the 15 cm flight tube, the time being varied by changing the ion acceleration voltage from 2 to 5 kV. In this series of measurements, particle size was kept constant at $\sim 4.1$ $\mu$m. For flight

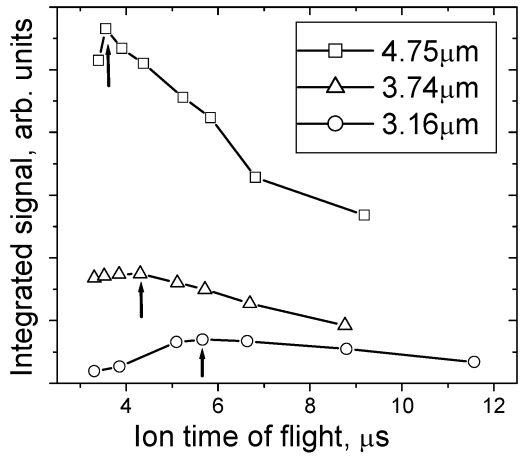


**Figure 7.** Integrated ion signal detected at the end of the 15 cm long TOF tube as a function of particle size for the same RbCl concentration of $3 \times 10^{-3}$ M. Note that the detector signals peak at different flight times, as indicated by the arrows.

times less than 4.3 $\mu$s, it is evident that the ion signal levels off. This flight time corresponds to a velocity perpendicular to the ion extraction axis of 3000 m/s and a kinetic energy of 3.8 $\pm$ 0.8 eV. Changes in the ion concentration had little effect on the derived kinetic energy. The maximum kinetic energies of the $Na^+$ ions (impurity) and the $Rb(RbCl)^+$ cluster ions were also found to be in the range of 3.0 and 3.5 eV. It appears then that the kinetic energy is independent of the ion concentration or the ion mass for a constant particle size.

If Coulomb explosion is the source of this ion kinetic energy, one might think that increasing the ion concentration would increase the final kinetic energy. However, as shown in the previous section, ion recombination reduces the initial ion concentration within 20 ns, during which time the ions cannot gain significant energy. In addition, during much of this time, the ion is surrounded by both negative and positive ions. Finally, the modeling shows that the final number of ions is independent of the ion concentration above a concentration of about $10^{-4}$ M. Nevertheless, it is possible to vary the number of ions by changing the particle size, keeping the ion concentration the same since the fraction lost due to ion-recombination depends only on the initial ion concentration. On the other hand, Coulomb repulsion, which is important only after the negative and positive ion clouds have separated and the vaporized particle has reached a size of about 400 $\mu$m, should increase with particle size because the total number of ions (after recombination) scales with the square of the diameter of the original particle. This increase in the kinetic energy is shown in Figure 7, where the integrated ion signal is plotted against the ion TOF. Here the onset of the plateau moves to shorter ion flight times as the particle size increases. Figure 8a shows the derived kinetic energy as a function of the integrated repeller current, which is a measure of the total number of ions. The RbCl concentration was held constant in these experiments at $3.2 \times 10^{-6}$ M. For the three particle sizes, 3.2, 3.7, and 4.8 $\mu$m, the maximum kinetic energies are 2.2, 3.7, and 5.5 eV, respectively. This trend indicates that larger Coulombic repulsive forces are present in the larger particles, a direct result of the larger number of ions in the larger droplets. The solid line in Figure 8a shows that the translational energy obtained from the Coulomb repulsion increases as the square root of the number of ions in the droplet.

The Langevin/Thomson ion-recombination model suggests that recombination stops after the particle reaches a size of about

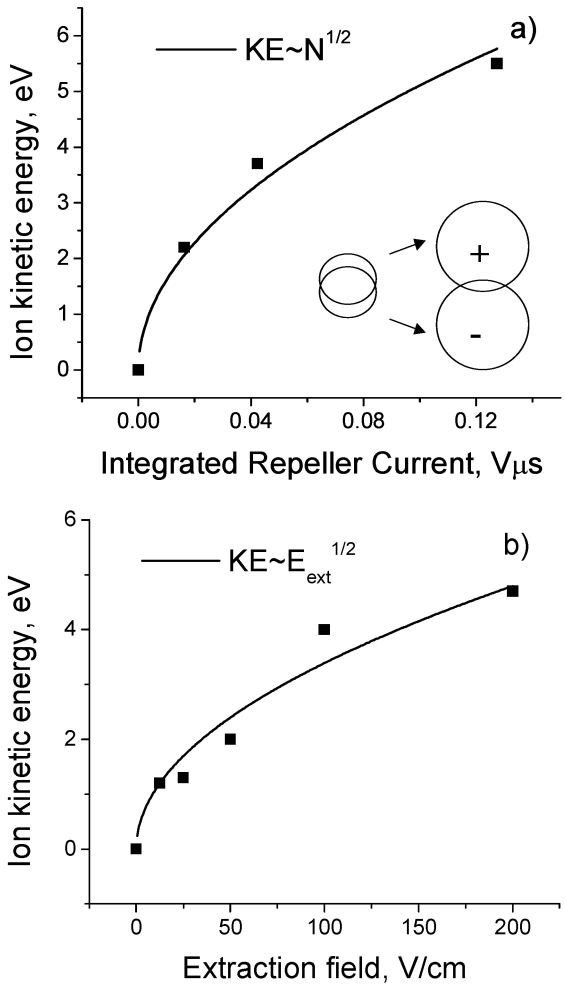


**Figure 8.** (a) Ion translational energy for three particle sizes, obtained from data in Figure 7, as a function of the integrated repeller current. The repeller current is a measure of the total number of ions detected. The solid line, which goes through the origin point, is a quadratic equation. (b) Ion translational energy as a function of the extraction field.

40 $\mu$m. However, at this point, the positive and negative ions are still in one cloud, as an overall neutral plasma held together by Coulombic forces between the negative and positive charges. If we assume that this cloud continues to expand at the sound velocity, the positive and negative charges will separate completely in the applied electric field when this field is larger than the Coulomb attraction of the positive and negative charges. We can crudely estimate that these two spherical clouds are completely separated (see inset in Figure 8a) when the electric field is just twice the Coulomb attraction field. That is

$$E_{\text{ext}} = 2\frac{Ne}{4\pi\epsilon_0 R^2} \tag{8}$$

where $E_{\text{ext}}$ is the external applied electric field, $N$ is the number of positive and negative ions, $e$ is the electron charge, and $R$ is the radius of the two clouds. For a droplet with $N = 10^6$ ions (after recombination) and an applied electric field of 200 V/cm, the radius of the two spheres when they are completely separated is calculated from eq 8 to be 400 $\mu$m.

To calculate the ion Coulomb repulsion energy, we suppose that the positive ions begin to repel each other only after the positive and negative clouds are completely separated (as shown in Figure 8a), and we further assume that the presence of the

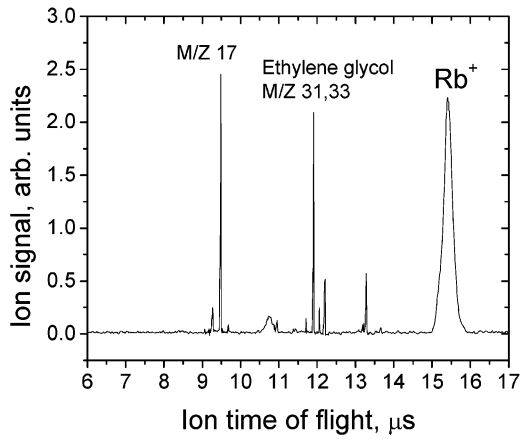


**Figure 9.** TOF mass spectrum of a RbCl in ethylene glycol droplet obtained by IR vaporization of the droplet followed by ionization of the neutral gas species by a vacuum UV laser pulse. Note the broad ion peaks arise from the IR laser evaporation while the narrow ethylene glycol peaks were generated by the VUV laser after the particle had expanded to a diameter of 1 mm.

negative ion cloud has no effect on the positive ion final kinetic energies. The final translational energy, found by integrating the Coulomb force from the radius $R$ to $\infty$, is then given by

$$KE_{[eV]} = \frac{Ne}{4\pi\epsilon_0 R} = \sqrt{\frac{NeE_{ext}}{8\pi\epsilon_0}} \qquad (9)$$

where we have substituted the value for $R$ in eq 8. This equation predicts that the final kinetic energy should be proportional to $N^{1/2}$, as found experimentally in Figure 8. Equation 9 also predicts a square root dependence of the ion energy on the extraction field, a dependence that is also confirmed experimentally in Figure 8b. The reason for the dependence on the electric field is that the greater the field, the smaller will be the separated ion clouds (see inset in Figure 8a) and thus the greater the Coulomb repulsion.

**Kinetic Energy Measured by Peak Broadening.** Figure 9 shows the TOF peak widths for the neutral species ionized with the vacuum UV laser after the gas cloud has expanded as well as the ion peak widths obtained when the IR laser alone vaporizes the ionic liquid droplet. Most of the narrow peaks (35 ns) are assigned to ionization of the ethylene glycol solvent. On the other hand, the two broad peaks are ascribed to the ions that were "liberated" by the IR laser pulse. The $Rb^+$ peak has a width of 370 ns. The origins of the TOF scale for these two classes of ions differ because the salt ions started their flight with the firing of the $CO_2$ (IR) laser, whereas the ethylene glycol ions started 2.4 $\mu$s later when the vacuum UV laser was fired.

The initial ion velocity, $v_0$, can be determined from the peak width by eq 10, in which the $\Delta$TOF is the difference in the TOF between two ions with the same speed, but ejected in opposite directions, namely toward and away from the ion detector.[28]

$$v_0 = \frac{eE_{ext}\Delta\mathrm{TOF}}{2m} \qquad (10)$$

where $m$ is the ion mass and the remaining variables are as before. The calculated velocity of the ethylene glycol fragment ions is 1000 m/s for both the $m/z$ 31 and 33 ions, which is much less than the 4200 m/s for the $Rb^+$ ions. In addition, the initial velocity obtained from the TOF peaks of $Na^+$, $Rb^+$, and $Rb_2Cl^+$ scale very nicely with $m^{-1/2}$, indicating that all of the ions have approximately the same initial kinetic energy.

Many MALDI studies have attributed the initial kinetic energies of the resulting ions to matrix entrainment in the expanding neutral species after laser ablation. In these studies, the measured velocities of the neutrals are typically similar to those of analytes, namely in the range of 100−1000 m/s.[29,30] The TOF spectrum in Figure 9 clearly shows that the initial velocity of the $Rb^+$ is not the result of entrainment in the rapidly expanding cloud of neutral solvent. Rather, we ascribe it to Coulomb explosion.

It is apparent that the $Rb^+$ velocity and kinetic energy determined from Figure 7 (3000 m/s and 3.8 ± 0.8 eV, respectively) are considerably lower than the velocity and energy of the $Rb^+$ ions determine from the peak width (4200 m/s and 7.7 eV). Because of the manner in which the negative and positive ion clouds separate during the expansion process, there is no reason that the Coulomb forces should be the same in the axial and equatorial directions. In fact, the difference can be attributed to ion cloud interaction and it is confirmed by computer simulation.

**Relationship to ESI and MALDI.** As pointed out in the Introduction, a number of analytical experiments suffer from a similar lack of sensitivity as the analyte concentration is raised. Is the ion−ion recombination mechanism proposed here responsible for this effect in all of these studies? The answer is not obvious, and it depends on a number of factors.

Although electrospray ionization is similar to our aerosol particle IR vaporization process in that both involve micron size droplets and convert preexisting aqueous ions into gas phase ions, there are some fundamental differences in the two processes. The droplets in ESI are highly charged, are created at 1 atm pressure and slowly evaporate over the period of several hundred microseconds. In contrast, our droplets are rapidly vaporized into a vacuum in less than 100 ns. As the ESI droplets shrink by slow solvent evaporation, the solvated ions remain in solution, in contrast to the ions in the present study that lose their solvent essentially instantaneously. As a result, the ions in the present study are lost by gas phase ion−ion recombination, whereas in ESI the bulk of the ions remain in solution and precipitate out as the droplet becomes supersaturated. The ions observed in ESI are those that are ejected from the highly charged surface. At low concentration essentially all of the solvated ions have a chance to reach the surface and eventually escape, but because of the limited surface area, this is not possible at higher concentrations.

The mechanism for the production of ions in MALDI is quite complex involving energy transfer from the matrix to the analyte molecules, and the production of both ionic and neutral species. Since the density of gas-phase ions (positive and negative) and neutrals is large, ion−ion recombination must diminish the number of ablated ions. A major difference between the aerosol and MALDI experiments is in the measured ion kinetic energies. In MALDI the ions are entrained in the expansion of the neutral species so that all ions have the same velocity, whereas in our aerosol experiment, the kinetic energy of the ions is determined by Coulomb explosion and is thus much higher than the kinetic energy of the neutral species. This difference is probably a result of the much greater mass of neutral species that are ablated in the MALDI experiment. Our aerosol sample size is a sphere of only 2−5 $\mu$m diameter, whereas in the MALDI experiment a much larger volume of sample is ejected. This results in high collision rates in the MALDI experiment and thus entrainment of the ions.

## Conclusions

This study discusses the importance of ion−ion interactions in laser desorption experiments. The experimental conditions are carefully controlled, using simple salt solutions of known volumes in size-selected particles. High laser powers are used to ensure that the particles are completely vaporized. A total ion current detector provides a measure of the absolute number of ions produced in the laser desorption process. The quantitative application of the Langevin/Thomson theory for ion recombination at various gas densities has positively identified ion−ion recombination as the most important mechanism for signal loss in aerosol mass spectrometry. Both the experiment and the model show that ion concentrations in excess of $3 \times 10^{-5}$ M are significantly depleted by ion recombination. For concentrations greater than $10^{-3}$ M, more than 99% of the ions are lost as a result of ion-recombination. The model predicts that the ion recombination proceeds for about 20 ns, at which time the aerosol particle (with an initial size of 1−4 $\mu$m) has been vaporized and the gas plume has reached a size of approximately 40 $\mu$m with an equivalent room-temperature pressure of about 1 atm. At later times, corresponding to lower gas densities, the ions are no longer depleted by ion recombination. On the other hand, once the plume of positive and negative ions are separated (at a plume diameter of about 400 $\mu$m in our experiment), Coulomb repulsion imparts significant kinetic energy to the ions, which may further reduce the ion signal.

**Acknowledgment.** We are grateful to the Air Force Office of Scientific Research and to the National Science Foundation for support of this work.

## References and Notes

(1) Woods, E., III.; Dessiaterik, Y.; Miller, R. E.; Baer, T. *J. Phys. Chem. A* **2001**, *105*, 8273.
(2) Enke, C. G. *Anal. Chem.* **1997**, *69*, 4885.
(3) Dreisewerd, K. *Chem. Rev.* **2003**, *103*, 395.
(4) Fenn, J. B. *J. Am. Soc. Mass Spectrom.* **1993**, *4*, 524.
(5) Poth, L.; Castleman, A. W. *J. Phys. Chem. A* **1998**, *102*, 4075.
(6) Zook, D. R.; Bruins, A. P. *Int. J. Mass Spectrom.* **1997**, *162*, 129.
(7) Tang, L.; Kebarle, P. *Anal. Chem.* **1995**, *65*, 927.
(8) Constantopoulos, T. L.; Jackson, G. S.; Enke, C. G. *Anal. Chim. Acta* **2000**, *406*, 37.
(9) Schoolcraft, T. A.; Constable, G. S.; Zhigilei, L. V.; Garrison, B. J. *Anal. Chem.* **2000**, *72*, 5143.
(10) Yingling, Y. G.; Zhigilei, L. V.; Garrison, B. J.; Koubenakis, A.; Labrakis, J.; Georgiou, S. *Appl. Phys. Lett.* **2001**, *78*, 1631.
(11) Johnson, R. E. Models for matrix-assisted laser desorption and ionization: MALDI. In *Large Ions: Their Vaporization, Detection and Structural Analysis*; Baer, T., Ng, C. Y., Powis, I., Eds.; John Wiley & Sons: Chichester, England, 1996; pp 49−77.
(12) Vertes, A. *Microbeam Anal.* **1991**, 25.
(13) Gluckmann, M.; Karas, M.;. *J. Mass Spectrom.* **1999**, *34*, 467.
(14) Mansoori, B. A.; Johnston, M. V.; Wexler, A. S. *Anal. Chem.* **1996**, *68*, 3595.
(15) Wattenberg, A.; Sobott, F.; Barth, H. D.; Brutschy, B. *Eur. Mass Spectrom.* **1999**, *5*, 71.
(16) Wattenberg, A.; Sobott, F.; Barth, H. D.; Brutschy, B. *Int. J. Mass Spectrom.* **2000**, *203*, 49.
(17) Sheffer, J. D.; Murray, K. K. *Rapid Commun. Mass. Spectrosc.* **1998**, *12*, 1685.
(18) Woods, E., III.; Smith, G. D.; Dessiaterik, Y.; Baer, T.; Miller, R. E. *Anal. Chem.* **2001**, *73*, 2317.
(19) Liu, P.; Ziemann, P. J.; Kittelson, D. B.; McMurry, P. H. *Aerosol Sci. Technol.* **1995**, *22*, 293.
(20) Liu, P.; Ziemann, P. J.; Kittelson, D. B.; McMurry, P. H. *Aerosol Sci. Technol.* **1995**, *22*, 314.
(21) Loeb, L. B. *Basic Processes of gaseous electronics*; University of California Press: Berkeley and Los Angeles, CA, 1955.
(22) Brown, S. C. *Basic Data of Plasma Physics*; John Wiley & sons: New York, 1959.
(23) Langevin, P. *Ann. Chim. Phys.* **1903**, *28*, 433.
(24) Thomson, J. J. *Philos. Mag.* **1924**, *47*, 337.
(25) Zeldovich, Ya. B.; Raizer, Yu. P. *Physics of Shock Waves and High-Temperature Hydrodynamic Phenomena*; Academic Press: New York, 1966.
(26) Woods, E., III.; Miller, R. E.; Baer, T. *J. Phys. Chem. A* **2003**, *107*, 2119.
(27) McDaniel, E. W.; Mason, E. A. *The Mobility and Diffusion of Ions in Gases*; Wiley: New York, 1973.
(28) Zelenyuk, A.; Cabalo, J.; Baer, T.; Miller, R. E. *Anal. Chem.* **1999**, *71*, 1802.
(29) Beavis, R. C.; Chait, B. T. *Chem. Phys. Lett.* **1991**, *181*, 479.
(30) Pan, Y.; Cotter, R. J. *Org. Mass Spectrom.* **1992**, *27*, 3.